PROCEEDINGS, 48th Workshop on Geothermal Reservoir Engineering
Stanford University, Stanford, California, February 6-8, 2023
SGP-TR-224

Hydraulic Fracturing in Petroleum and Geothermal Reservoirs with Reference to the Utah FORGE Stimulation

Ahmad Ghassemi and Dharmendra Kumar

Reservoir Geomechanics and Seismicity Research Group, The University of Oklahoma, Norman, OK, USA

ahmad.ghassemi@ou.edu

Keywords: Geothermal, Hydraulic Fracturing, Hydraulic Stimulation, Rock Anisotropy, Unconventional Geothermal Reservoirs, EGS

ABSTRACT

In this paper, we present some fundamental aspects of hydraulic fracture height growth in unconventional petroleum and geothermal reservoirs and describe the likely shape of the hydraulic fracture or the stimulated reservoir volume (SRV) resulting from the Stage 3 stimulation in the Utah FORGE. We use a 3D poroelastic DD method which considers planar and non-planar fracture propagation and interactions with natural fractures. We show that asymmetric height growth is to be expected in the stress regimes encountered in EGS and that height growth can be hindered by the rock mass discontinuities such as preexisting fractures, rock anisotropy, and lithological boundaries. In the case of Stage 3 in Utah FORGE, the data seems to suggest upward growth and interaction with natural fractures, leading to a moderately complex SRV consisting of a HF/NF network.

1. INTRODUCTION

Hydraulic fracturing technology which is extensively used in unconventional petroleum reservoirs has gained popularity in EGS or what we have termed "unconventional geothermal reservoirs" (Ghassemi, 2021). However, the geometry of hydraulic fractures in EGS which is crucial for well stimulation is still not adequately understood, and recently, several reservoir creation concepts have been proposed for alternative EGS development based on conceptual models from petroleum reservoirs where rock type and stress regimes have historically favored planar hydraulic fracture with significant length and limited height growth (in a few cases unusual height growth is observed in the Delaware basin based on fiber data, although there could be alternative interpretations for the strain signature used to suggest the 1000-1500 ft. height. We examine the condition that controls hydraulic fracture geometry and showed that in geothermal reservoirs, the preferential growth direction is upwards resulting in relatively short length unless natural preexisting discontinuities and novel growth control mechanism takes advantage of to encourage lateral extension. We use a 3D fully coupled model for the hydraulic fracture simulation using a combination of the displacement discontinuity (DD) method for the rock mass deformation and the finite element method for the fluid flow modeling. The fracture propagation is implemented in the framework of the linear elastic fracture mechanic approach. The fracturing fluid is assumed incompressible and follows the Newtonian behavior. The rock matrix is assumed linear elastic/poroelastic, with constant physical properties.

2. NUMERICAL MODELING

The simulation modeling approach builds on previous work we have carried out on the simulation of the hydro-mechanical response of fractures and fractured reservoirs reservoir rocks (e.g., Zhou and Ghassemi, 2011; Ghassemi et al., 2013; Safari and Ghassemi, 2016; Kumar and Ghassemi, 2016 & 2018). Details of the numerical implementation and the coupled solution procedures used in this paper can be found in Ghassemi et al. (2013) and Kumar and Ghassemi (2016 and 2018). The fracture propagation process is analyzed in the framework of linear elastic fracture mechanics (LEFM). The modified 3D maximum circumferential criterion as suggested by Schöllmann et al. (2002) is used for the mixed-mode fracture propagation analysis, and the fracture propagation growth is determined using scaling (Mastrojannis et al. 1980; Kumar and Ghassemi 2016 and 2018). The interaction between the HF and NF is accounted for using the procedures described in Kamali et al. (2022) which uses a crossing criterion (Gu and Weng, 2010; Gu et al. 2012) based on the tendency of the natural fracture to slip; crossing occurs when the resultant shear stress on the interface is such it does not initiate slip. Various components of the model have been verified as described in the sources cited in the preceding paragraph.

3. Expected Hydraulic Fracture Geometry in Petroleum & Geothermal Settings

The reservoir conditions in geothermal settings vary widely from those in petroleum reservoirs. The latter occurs in layered sedimentary systems where different rock properties above and below the target zone tend to have larger lateral stress magnitudes, thereby hindering upward hydraulic fracture growth. As can be seen in Figure 1a, a strong stress barrier causes the fracture to be contained and attain larger lateral growth. In contrast, a weak stress barrier promotes more height growth, as shown in Figure 1b. If multiple fractures are placed close to each other, the competition between the fractures and the stress shadow (and perforation erosion) would determine the extent of upward or lateral growth, as shown in Figure 2.

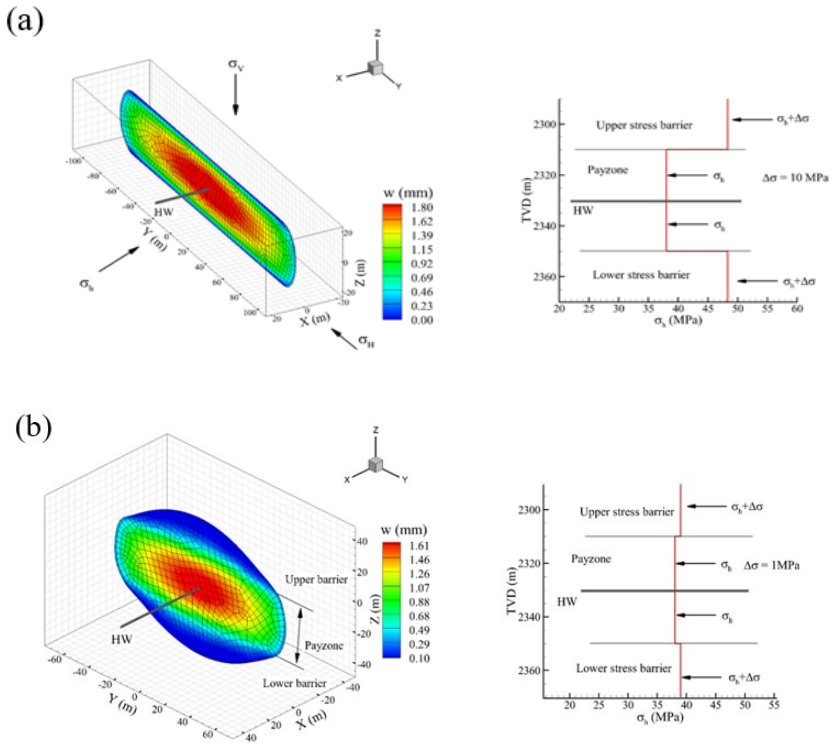

Figure 1. 3D Propagation of a single hydraulic fracture in a shale reservoir with different stress barrier conditions (for input parameters, see Kumar and Ghassemi, 2020).

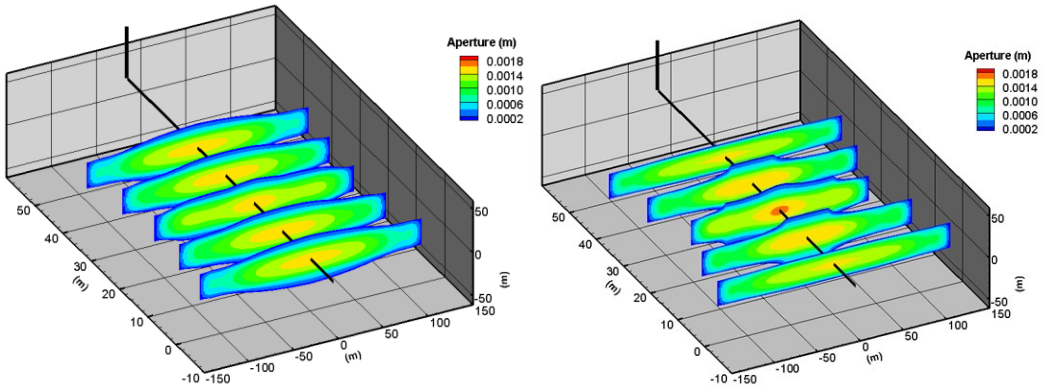

Figure 2. Multi-stage stimulation in a shale reservoir with different stress barrier magnitudes of Δσ= 1 MPa (left), Δσ= 3 MPa (right) with no leak-off. Fluid viscosity of 1 cP, elastic modulus of 35 GPa, Poisson's ratio of 0.25; rock fracture toughness of 1.5 MPa m $^{0.5}$. The injection rate is 80 bbls/min using a fluid with a density of 8.33 lbm/gal and 1 cp viscosity. The perforation diameter is 0.3 inches without erosional effects (see Sesetty and Ghassemi, 2019).

In contrast, a stress barrier is often lacking in EGS settings, such that the hydraulic fracture tends to grow upward, with much less than expected lateral growth tendency. As an example, consider the stimulation of Well 55-29 in Newberry reservoir, which is being considered for a superhot EGS project. Details of the reservoir properties can be found in Wang et al. 2016. A summary of the relevant properties is shown in Table 1.

3.1 The Role of Rock Anisotropy

The impact of rock anisotropy on fracture height growth has been studied by Sesetty and Ghassemi (2018). They have found that isotropic fracture models tend to overestimate the fracture height and underestimate fracture width. In addition, the fracture width of multiple fractures tends to be more uniform in anisotropic rock compared to the isotropic case and there is a substantial increase in the stress shadow for anisotropic rock even for a low degree of anisotropy of nearly 2 (see Figures 3, and 4). It should be noted that height growth

can also be impeded by layer's mechanical properties and their interfaces. For a comprehensive analysis, the reader is referred to Gao and Ghassemi (2020, 2021).

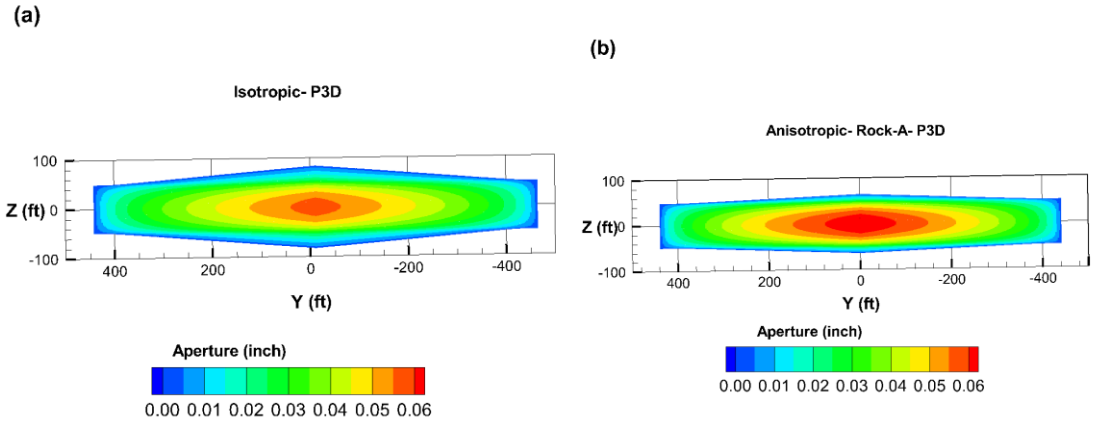

Figure 3: Comparison of (a, b) fracture geometry for isotropic and anisotropic models for a single planar fracture (from Sesetty and Ghassemi, 2018a, b).

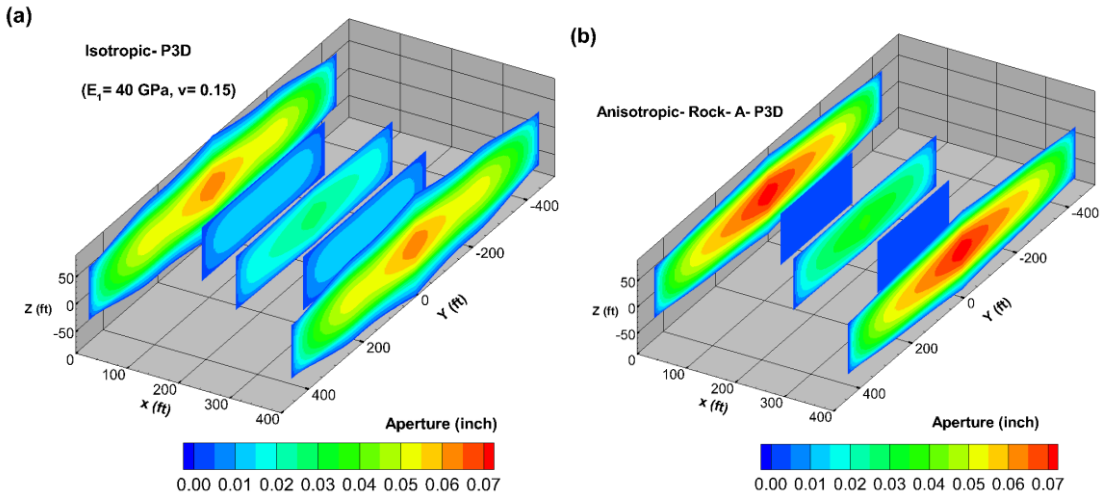

Figure 4: Comparison of fracture geometry and aperture distribution for simultaneous propagation of fractures from multiple clusters, (a) isotropic rock and (b) anisotropic rock (Rock-A) with 90 ft cluster spacing and 1 MPa additional stress barrier in the bounding layers (from Sesetty and Ghassemi, 2018 a,b). E_1= E_2=40 GPa, E_3=10 GPa, ν_{12}=0.15, ν_{13}=0.185, G_{13}=7.45 GPa, K_{IC}=1.5 MPa.m$^{1/2}$.

3.2 Expected Hydraulic Fracture Geometry in Geothermal Settings

For a single stage stimulation in the Newberry reservoir at a depth of 3000 m, assuming that no discontinuities are present on its path, the resulting hydraulic fracture geometry is shown in Figure 5 (for an injection rate of 30 bbls/min). As can be seen in Figure 5a, the hydraulic fracture tends to grow upward with decreasing lateral extent. To mitigate the excessive height growth, one may consider using a denser fracturing fluid. However, as can be seen in Figures 5a, 5b, and 5c, the impact is not significant in this case of reservoir minimum stress gradient.

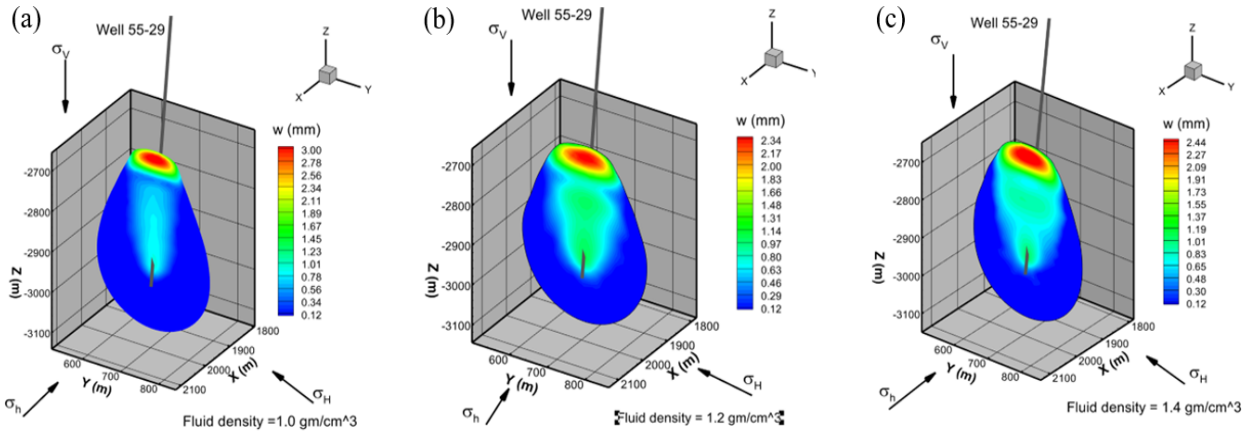

Figure 5: Hydraulic fracture geometry in Newberry superhot project when no discontinuities are considered in the simulation. Left to right: increasing fracture fluid density.

On the other hand, in the presence of discontinuities such as natural fractures are considered in the simulations, a rather different fracture propagation path is observed (Figure 6). In this case, the characteristics of the discontinuities such as natural fracture size, spacing, and surface properties exert control over the hydraulic fracture geometry. For a sparse fracture spacing, the hydraulic fracture continues its upward growth but attains an irregular geometry where the top portion is wider than its lower segment. The intersection with NFs increases the pore pressure in the natural fractures, causing them to dilate. Note that when the HF intersects the NFs fluid leak-off dilates the natural fractures. When the NF spacing is less, the HF is trapped and cannot attain height. And if the HF cannot cross the natural fractures in the lateral direction, it remains trapped and continued injection at even higher rates (60 bbls/min) significantly pressurizes the NFs causing them to open.

Table 1: Input parameters for Newberry Superhot EGS.

Parameter	Value
E (GPa)	27.2
v (-); v_u (-)	0.36; 0.45
Biot's coefficient; porosity	0.5; 3.24%
σ_{hmin} (MPa/m)	0.0149
σ_{Hmax} (MPa/m)	0.0235
σ_V (MPa/m)	0.0241
K_n^* (GPa/m)	100.0
K_s^* (GPa/m)	100.0
$w_{0_{NF}}$ (mm)	0.5
ϕ_{NF} (°), Cohesion, MPa	45; 1.0
Fluid Viscosity (Pa. sec)	1.0709×10^{-4}
Carter's Leak-off coeff. (m/s$^{0.5}$); Matrix permeability (mD);	$1.575\text{x}10^{-5}$; 5×10^{-4}

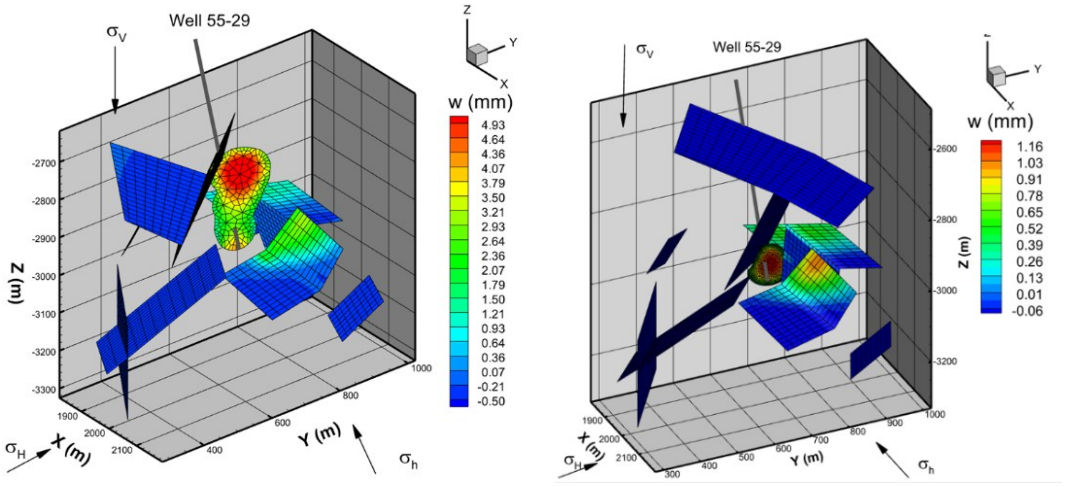

Figure 6: (a) Hydraulic fracture geomtry in Newberry superhot project for a sparse NF realization, after 25 min of pumping at 30 bbls/min (left). (b) HF growth through closely-spaced NFs. The NFs stress shadow and leak-off suppress HF growth (right).

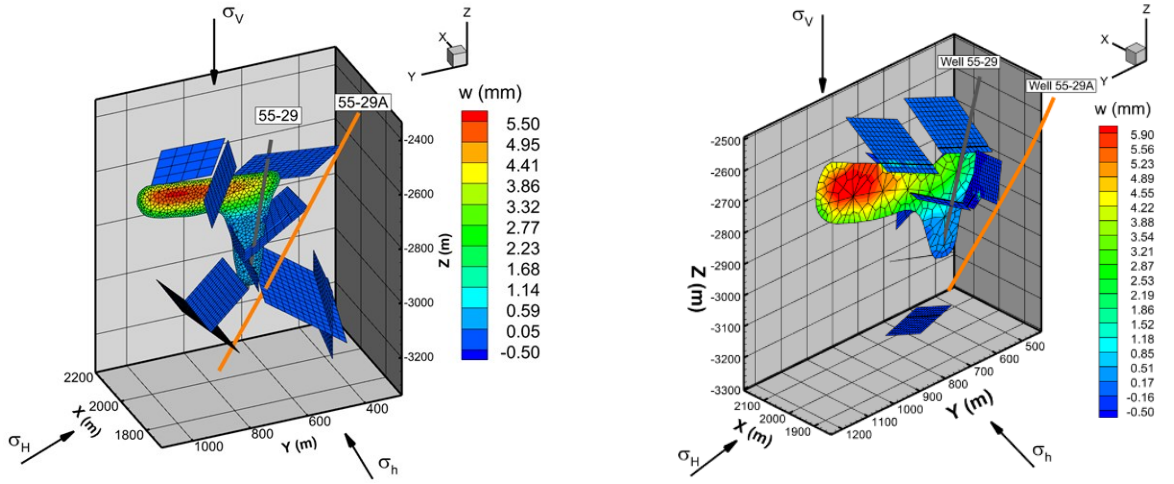

Figure 7: Left: Hydraulic fracture grows up through lower level NFs and is caged atby NFs at shallower depths. Right: Sparse NF at depth with crossing conditions/ Injection volume of 2232.36 bbls. with 20% leak-off in both cases.

When the HF is allowed to cross the NFs in its close vicinity, some height growth is observed (Figure 7). However, termination of shallower NFs forces the Hf to grow in the lateral direction as it seeks the zone of low NF stress shadow and turns to the left. In the case of higher-density NF occurrence, the HF/NF interaction becomes stronger, as shown in Figure 7 (left). In this case, the HF is trapped by a suitably oriented NF, terminating its upward growth. With continued injection (30 bbls /min of 0.11 cp fluid for 66 min) the HF is forced to grow asymmetrically in the lateral direction. In the case of a modified DFN configuration (right), the HF size is larger at depth and once it passes through the zone of stress influence of the shallow NF, it gains an upward growth tendency once again. Such complex interactions have a significant impact on the trajectory of the second well (producer). Clearly, data on the DFN configuration in the reservoir is not readily available. But recording seismicity during stimulation can provide insight regarding the fracture growth evolution and combined with numerical modeling, can assist in the optimum planning of the second well. The case of Utah FORGE stimulation underscores this point.

4. Numerical Modeling of the Stage 3 Stimulation in Utah FORGE Well 16A (78)-32

In this section, we model Stage-3 hydraulic stimulation of Well 16A (78)-32. Figure 8 illustrates the simulation domain. The natural fractures geometry has been obtained from the FORGE Geothermal Data Repository and used to generate an equivalent continuum permeability distribution (left). The actual discrete fracture network (DFN) distribution around the wellbore used in the HF simulation is shown on the rights. The DFN shown is a subset of the DFN chosen based on its potential for interacting with the HF from the perforated interval. In addition, a few additional NFs are added to allow for sufficient leak-off to satisfy the mass balance requirements for the long injection time. The input parameters used for FORGE stimulation modeling are listed in Table 2, and the initial pressure and temperature used are provided by Native Stage FALCON input data from Idaho National Laboratory. We re-examined impact of fluid density on the fracture growth pattern for the FORGE case as shown in Figure 8 (upper part) and found that if the fluid's unit weight is higher than the slope of the minimum in-situ stress, we can limit upward growth of hydraulic fracture up to some extent. The injection and the planned production well in a continuum representation of the rock mass shown in lower left of Figure 8 and the DFN used in modeling of HF from Stage-3 perforated interval is shown in lower right of Figure 8.

Table 1: Input parameters Stage 3 Stimulation Modeling

Parameter	Value
E (GPa)	54.6
v (-)	0.29
σ_{hmin} (MPa/m)	0.0165
σ_{Hmax} (MPa/m)	0.0218
σ_{V} (MPa/m)	0.0256
K_n^* (GPa/m)	100
K_s^* (GPa/m)	100
$w_{0_{NF}}$ (mm)	0,5
ϕ_{NF}^* (°)	45
Fluid viscosity (cp)	1.0
Carter's Leak-off coeff. ($m/s^{0.5}$)	$1.575x10^{-5}$

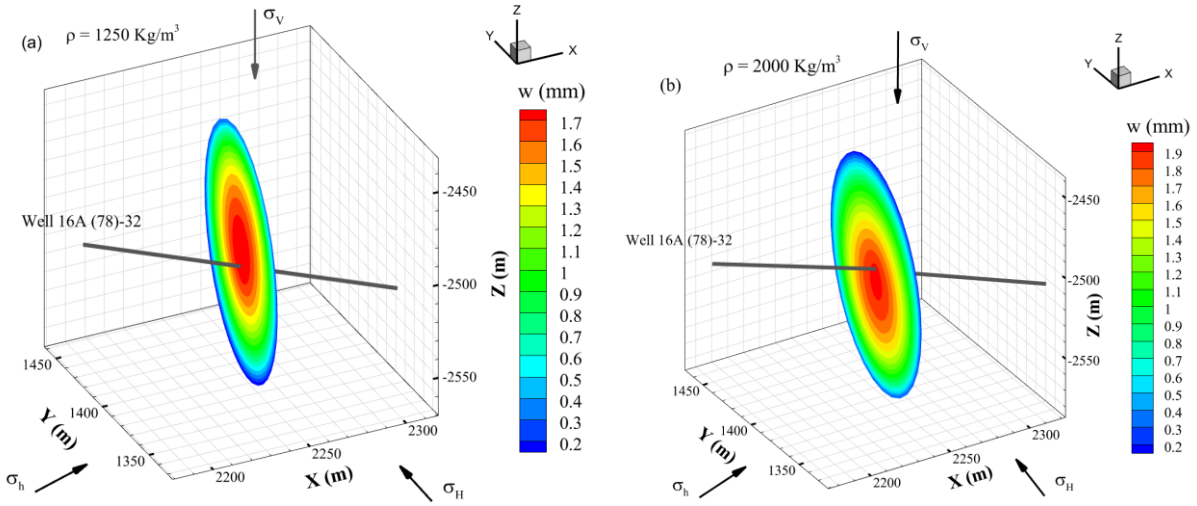

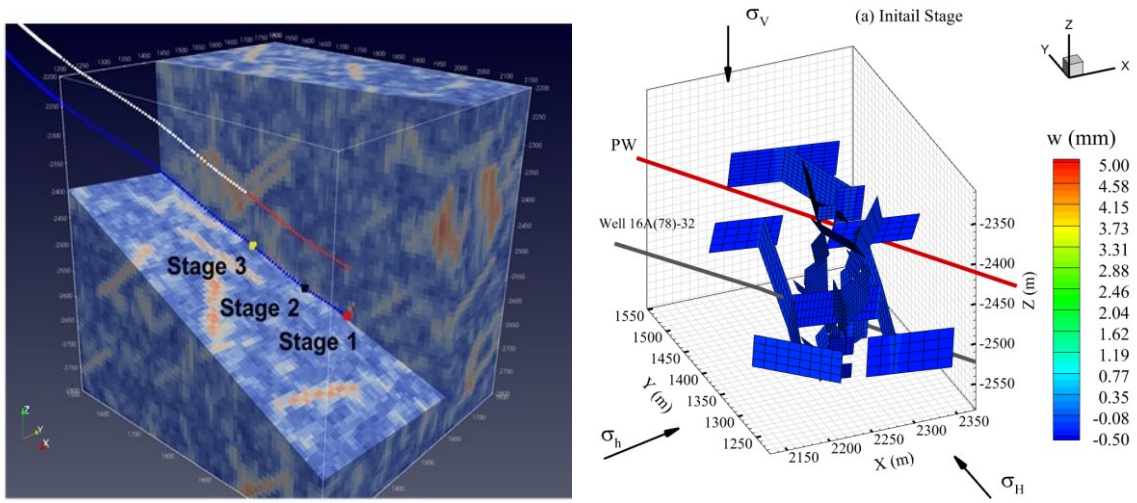

Figure 8: Impact of fluid density on the hydraulic fracture propagation (upper part). The injection and the planned production well in a continuum representation of the rock mass (lower left). The DFN used in modeling of HF from Stage-3 perforated interval (lower right).

time (min)	Injenction rate (bpm)
0.00	5.000
12.09	5.000
16.97	8.075
23.14	12.516
28.72	16.374
39.30	19.890
75.55	24.032
106.58	27.699
116.67	15.937
126.42	12.572
131.41	8.382
136.99	4.309
139.77	0.232

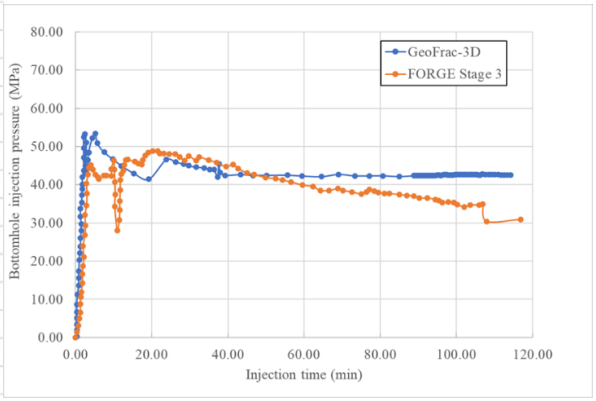

Figure 9: Pumping schedule used in the simulation. Comparison of the pressure record from the field and the numerical simulation.

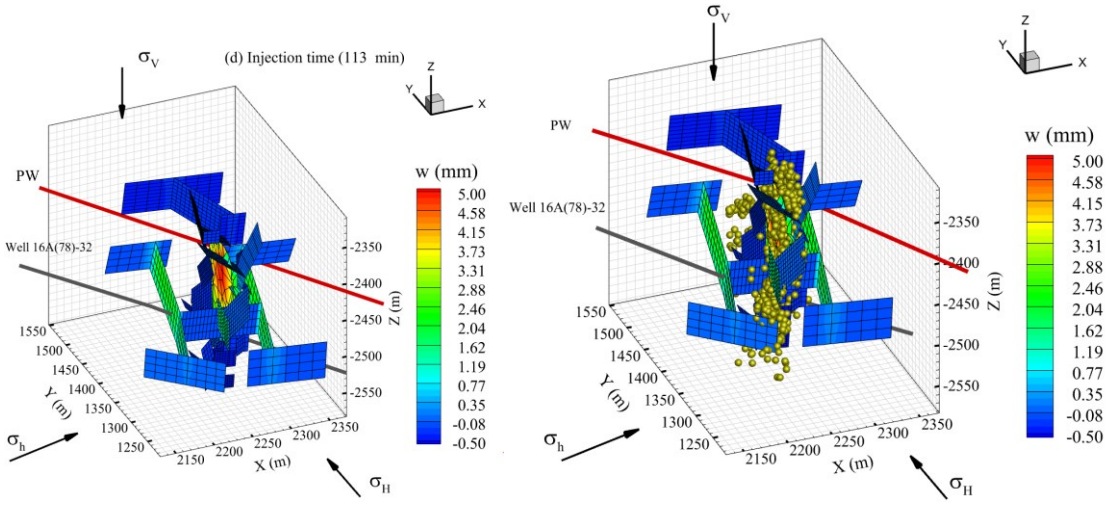

Figure 10: Numerical model results of hydraulic fracture growth. The right figure superimposes the seismicity data on the DFN and the HF.

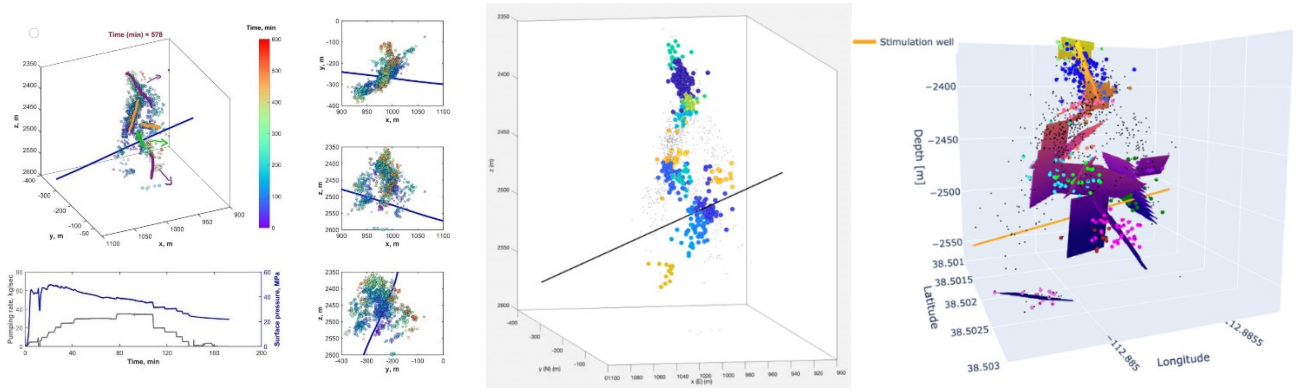

Figure 11: Left: Stage 3 seismicity data and visual plane fit (Ghassemi and Zhi (Quarterly report to FORGE, 1/31/2023). DBSCAN algorithm for automatic distance-based clustering of the microseismic events recorded during Stage 3 stimulation in April 2022 (middle) from Ghassemi and Chen (Quarterly report to FORGE, 1/31/2023). Principal component analysis was used to determine the fault plane for each of the clusters (right).

The numerical simulation results conform well with the DFN used in the simulations. However, as can be seen in Figure 11 (left) the stimulation may have involved a more complex process of fracture propagation such as wing crack formation. It is likely that a better match can be achieved using the planes identified from cluster analysis and considering the more detailed analysis of DFN propagation. Work in this direction is underway.

5. CONCLUSIONS

Features of hydraulic fracture propagation have been demonstrated for both petroleum and geothermal settings. In particular, the role of stress barrier, rock anisotropy and natural fractures have been illustrated with respect to fracture containment. In addition, a series of 3D hydraulic fracture simulations have been performed for Stage 3 stimulation in Utah FORGE EGS. The simulations have been adjusted by considering additional NFs and varying their size and apertures. As a result, we have been able to obtain a meaningful simulation time and pressure record. The findings underscore the significant impact of natural fractures on hydraulic fracturing in EGS and the need to design the fracturing jobs using more advanced modeling capabilities.

ACKNOWLEDGEMENTS

This project was supported by the Utah FORGE project sponsored by the U.S. Department of Energy, through the project "Application of Advanced Techniques for Determination of Reservoir-Scale Stress State at Utah FORGE" and "Experimental Determination and Modeling-Informed Analysis of Thermo-poromechanical Response of Fractured Rock for Application to Utah FORGE." The support of Alta Rock Energy for the Newberry fracturing project is also appreciated.

REFERENCES

Gao, Q., Ghassemi, A. 2021. The Impact of Layering and Permeable Frictional Interfaces on Hydraulic Fracturing in Unconventional Reservoirs. SPE Prod. & Operations, 36(4), 912-925. 10.2118/195881-PA.

Gao, Q., Ghassemi, A. 2020. Height Growth in Layered Unconventional Reservoirs: The Impact of Moduli, Interfaces and In-situ Stress. SPE Production & Operations SPE-201104-PA. https://doi.org/10.2118/201104-PA.

Ghassemi, A., Zhou, X., and Rawal, C. A three-dimensional poroelastic analysis of rock failure around a hydraulic fracture. *J. of Petro. Sci. & Eng*., Vol. 108 (2013),118-127.

Gu. H. and Weng, X. 2010. Criterion for fracture crossing frictional interfaces at non-orthogonal angles. 44th US Rock Mechanics Symposium and 5th U.S.-Canada Rock Mechanics Symposium, Salt Lake City, UT, June 27-30, 1-6.

Gu, H., Weng, X., Lund, J. B., Mack, M. G., Ganguly, U., & Suarez-Rivera, R. (2012). Hydraulic fracture crossing natural fracture at nonorthogonal angles: a criterion and its validation. SPE Production & Operations, 27(01), 20-26.

Kamali, A., Ghassemi, A., & Kumar, D. 2022. 3D Modeling of hydraulic and natural fracture interaction. *Rock Mech Rock Eng*.,1-19. https://doi.org/10.1007/s00603-022-03029-w

Kumar, D. and Ghassemi, A. A three-dimensional analysis of simultaneous and sequential fracturing of horizontal wells. J. of Petrol. Sci. Eng., Vol.146 (2016), 1006-1025.

Kumar, D. and Ghassemi, A. A three-dimensional poroelastic modeling of multiple hydraulic fracture propagation from horizontal wells. Int. J. of Rock Mech. and Mining Sci., Vol.105 (2018), 192-209.

Kumar, D. and Ghassemi, A. 2020. A fully coupled 3D simulation of hydraulic fracture networks propagation from the horizontal wells. Rock Mechanics for Natural Resources and Infrastructure Development –Fontoura, Rocca & Pavón Mendoza (Eds). ISRM, 2020.

Mastrojannis, E.N., Keer, L.M., and Mura, T. Growth of planar cracks induced by hydraulic fracturing. *Int. J. Numer. Methods Eng*., Vol. 15(1) (1980), 41-54.

Safari, R., and Ghassemi, A. Three-dimensional poroelastic modeling of injection induced permeability enhancement and micro-seismicity. Int. J. of Rock Mech. and Mining Sci., Vol. 84 (2016), 47-58.

Schöllmann, M., Richard, H.A., Kullmer, G., and Fulland, M. A new criterion for the prediction of crack development in multi-axially loaded structures. *Int. J. of Fract*. Vol.117 (2002), 129-141.

Sesetty, V., Ghassemi, A. 2019. Modeling Dense-Arrays of Hydraulic Fracture Clusters: Fracture Complexity, Net Pressure and Model Calibration. Urtec. DOI:10.15530/urtec-2019-1128.

Sesetty, V. K., Ghassemi, A. 2018a. Effect of rock anisotropy on wellbore stresses and hydraulic fracture propagation. Int. J. Rock Mech., 11, 369-384.

Sesetty, V. K., Ghassemi, A. 2018b. The Impact of Formation Anisotropy on Cluster Spacing in Horizontal Wells Using a New P3D Model. URTeC: 2878152.

Wang, J., Woodong, J., Li, Y., and Ghassemi, A. 2016. Geomechanical characterization of Newberry Tuff. Geothermics Special Issue on EGS. doi: 10.1016/j.geothermics.2016.01.016.

Zhou, X., and Ghassemi, A. Three dimensional poroelastic analysis of pressurized natural fracture. *Int. J. Rock Mech. and Mining Sci*., Vol. 48 (2011), 527-534.